A Wireless Power Transfer System With High Misalignment Tolerance and Low Component Count

Houji Li, *Student Member, IEEE*, Zhan Liu, *Student Member, IEEE*, Bo Pan, Wei Liu, *Graduate Student Member, IEEE*, Jian Wang, Ming Liu, *Senior Member, IEEE*, and Yong Wang, *Member, IEEE*

***Abstract*—To improve the misalignment tolerance of wireless power transfer (WPT) systems, two or more transmitting coils are generally required with independent control. The independent control of multiple coils usually needs the multiple inverters or additional switches, which increases the size and component count of the WPT system. In this article, a WPT system with novel TX coil driving circuit is proposed for high misalignment tolerance and low component count. The proposed circuit allows a single inverter with only two switches to control the magnetic field of two TX coils independently, which helps achieve the low component count and compact size. In the propose WPT system, two decoupling square coils are adopted as the bipolar transmitter and each of the coil is driven by one switch. When the receiving coil is misaligned, the two coils of the transmitter can distribute the output power according to the different positions of the receiving coil by the proposed driving circuit, thus ensuring a fixed total output voltage, namely high misalignment tolerance. Moreover, the detailed theoretical analysis and design approach are given in this article and the proposed circuit is compared with the existing approaches. A 1 MHz WPT prototype is built for verification purpose, and the constant output voltage can be achieved within a coil misalignment of −6 to 10 cm.**

***Index Terms*—High misalignment tolerance, low component count, two-coil driving circuit, zero voltage switching.**

I. Introduction

WIRELESS power transfer (WPT) is the technology with great potential, makes the transmission methods and applications of electric energy more diverse and extensive [1]. WPT technology can use magnetic field, electric field, microwave, laser, and other means of transmit power without external physical connections. At present, WPT is widely used in electric vehicle [2], [3], portable devices [4], medical [5], rail transportation [6], aerospace [7], ocean exploration [8], and household appliances [9], because of its high security, convenience, flexibility, and unnecessity of bulky cable and heavy plugs.

Currently, most of the WPT systems adopt magnetic field coupling method, i.e., two coils transmit energy through magnetic coupling. The shape, size, and position of the two coils will affect the strength of the magnetic coupling, which will affect the transmission capability of the WPT system. Generally, the magnetic coupling of the two coils is strongest when they are aligned. However, misalignment between the two coils is almost inevitable in a real WPT application, which may result in poor energy transfer capacity and efficiency [10], [11]. In order to improve the misalignment tolerance of the WPT system, many works are discussed, e.g., the coupling coils with uniform magnetic coupling, circuit topologies, and control methods for constant output, among, which the most straightforward way is optimizing the coupling coils. Pang et al. [12] discussed a double D (DD) coil with the same current direction between two D coils, which produces a single-sided flux, which is twice as large as the flux of a circular coil. However, the magnetic field type of the DD coil results in ineffective energy transfer at some position of the coil, i.e., null power point. To solve this issue, a spatial quadrature coil is added to the DD coil, named the DD quadrature (DDQ) coil [13], which can pick up the polarized flux generated by DD coil. However, the DDQ coils require the complex coil structure and driving circuit design, and low material utilization. In [14], a decoupled multicoil structure, namely bipolar (BP) coil, is introduced, which has the same characteristics as DDQ coil. Compared to DDQ coil, BP coil exhibits better interoperability features with improved material utilization and is simple to drive due to the identical coil structure. In addition, there are quadruple D (QD) [15], QD quadrature (QDQ) [9], DD two quadrature (DD2Q) [16], tripolar pad [17], and multicoil structures with high misalignment tolerance in multiple directions.

For the abovementioned high misalignment WPT design with multiple coils, multiple inverters are usually required to control the coils independently to generate the magnetic field properly, resulting in high component count and cost, large circuit size, and low reliability of the system. Li et al. [18] presented a wireless charging system based on compact and integrated double-sided decoupled coils, which adopting two transmitter and receiver. In [19], a decoupling control method is proposed so that two WPT power modules can achieve independent output

Manuscript received 31 March 2023; revised 17 July 2023 and 19 August 2023; accepted 24 September 2023. Date of publication 11 October 2023; date of current version 26 January 2024. This work was supported in part by the Natural Science Foundation of Shanghai under Grant 21ZR1431100 and in part by the Power Electronics Science and Education Development Program of Delta Group and Natural Science Foundation of China under Grant 52277194. Recommended for publication by Associate Editor M. Amirabadi. *(Corresponding author: Yong Wang.)*

The authors are with the Department of Electrical Engineering, Shanghai Jiao Tong University, Shanghai 200240, China (e-mail: lihoushen@sjtu.edu.cn; worldhuman@sjtu.edu.cn; panbost@sjtu.edu.cn; liuwei78@sjtu.edu.cn; wj1071268395@sjtu.edu.cn; mingliu@sjtu.edu.cn; wangyong75@sjtu.edu.cn).

Color versions of one or more figures in this article are available at https://doi.org/10.1109/TPEL.2023.3323420.

Digital Object Identifier 10.1109/TPEL.2023.3323420

control and, thus, be free from cross-coupling effects. However, these methods use separate inverters to control each coil independently, which may increase WPT system complexity and component count. To reduce the use of inverters and devices, an input-parallel single-switch wireless power transfer system is present in [20], which allows each coil to be controlled individually by one switch. Zhang et al. [21] introduced a novel quadrature coil and a converting circuit, which allows the coupler structure to be adjusted according to the relative position of the coils on both sides. This scheme adjusts the two identical DD coils overlapping 90° by means of a control switch to operate at optimum efficiency or power. In [22], a series of hybrid topologies are proposed, in which two coils are connected in series or in parallel within the same resonant circuit. This approach allows one full-bridge inverter to exploit the difference in the effect of mutual inductance on the output, thus achieving a constant output over a wide range. Ge et al. [23] proposed a dual-independent-output inverter, which can drive two coils independently by two controllable outputs. However, these circuits have one of the problems, such as additional components requirement, high voltage stress of switch, high complexity, incapability for independently multicoil control.

Therefore, design of a WPT system with high misalignment tolerance and simple coil-driving circuit is of great significance. In this article, a WPT system with novel TX coil driving circuit is proposed for high misalignment tolerance and low component count. The proposed circuit allows a single inverter with only two switches to control the magnetic field of two TX coils independently, which helps achieve the low component count and compact size. In the propose WPT system, two decoupling square coils are adopted as the bipolar transmitter and each of the coil is driven by one switch. When the receiving coil is misaligned, the two coils of the transmitter can distribute the output power according to the different positions of the receiving coil by controlling the two switches, thus ensuring a fixed total output voltage, namely high misalignment tolerance. Compared with the half bridge topology, the proposed circuit can drive two coils and control their power independently for high misalignment tolerance by only two switches. Compared with the single switch topologies, e.g., the Class E inverter, the proposed circuit has no need of inductors and lower switch voltage stress due to its Qusi-square wave drain source voltage.

This article presents the operating modes, power distribution control, misalignment characteristics, ZVS operation, and parameter design of the proposed WPT system and coil driving circuit. The system performance with varying load condition and coil misalignment is investigated theoretically and experimentally, and the proposed circuit is compared with other schemes in terms of misalignment tolerance and component count, to validate the advantages of the proposed WPT system and circuit.

II. Proposed TX Coil Driving Circuit

A. Circuit Topology

In this article, a novel TX coil driving circuit is proposed for WPT application, which allows a single inverter with only two switches to control the magnetic field of two TX coils independently, as shown in Fig. 1. Here, the compensation network L_{T1}-C_{T1} and the low-side switch Q_1 form a single-switch LC circuit to drive the transmitting coil L_{T1}, the high-side switch Q_2 and clamp capacitor Cc form another single-switch branch to drive the transmitting coil L_{T2} with the compensation network C_2-L_{T2}-C_{T2}. Due to the compensation networks L_{T1}-C_{T1} and C_2-L_{T2}-C_{T2}, the switches Q_1 and Q_2 can also achieve the low dv/dt operation, which is very similar with the operation of single-switch Class E topology but with much lower switch voltage stress compared with Class E topology.

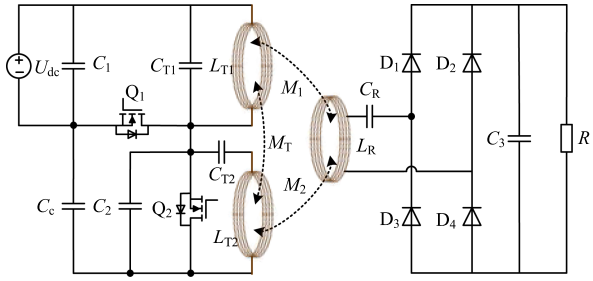

Fig. 1. Proposed TX coil driving circuit for WPT system.

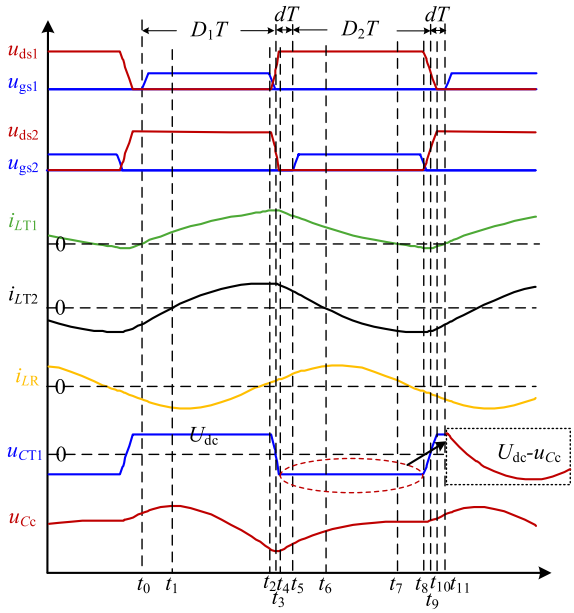

Fig. 2. Key waveforms of the proposed two-coil driving circuit.

As shown in Fig. 1, the two transmitting coils L_{T1} and L_{T2} can be independently controlled by adjusting the duty cycle and phase of the low-side and high-side switches, and the two coils worked as a decoupled bipolar transmitter. Here, the M_1 and M_2 are the mutual inductances between transmitting coils (L_{T1} and L_{T2}) and receiving coil (L_R), and M_T is the cross-coupling between two transmitting coils, which is neglectable due to the decoupled coil structure. And C_R is the compensation capacitor of the receiving coil.

The key waveforms of the proposed two-coil driving circuit are shown in Fig. 2. Here, u_{gs1} and u_{ds1} are the gate-source

voltage and drain-source voltage of Q_1, u_{gs2} and u_{ds2} are the gate-source voltage and drain-source voltage of Q_2, i_{LT1} and i_{LT2} are the current of the transmitting coil L_{T1} and L_{T2}, i_{LR} is the current of the receiving coil L_R, u_{CT1} and u_{Cc} are the voltage of compensation capacitor C_{T1} and clamp capacitor Cc, D_1 and D_2 are the duty cycle of Q_1 and Q_2, T is the switching period, and d is the dead time. As shown in Fig. 2, the proposed circuit can achieve ZVS turn ON and low dv/dt operation of two switches.

B. Operation Principle

The operation process of the proposed two-coil driving circuit can be divided into 11 modes, as shown in Fig. 3. It can be given as follows.

Model 1 *[t_0-t_1]:* At time t_0, the gate-source voltage u_{gs1} becomes a high level, the low side switch Q_1 is turned ON. With the input voltage charges the transmitting coil L_{T1} through Q_1, the current of the transmitting coil L_{T1} gradually rises from zero. The transmitting coil L_{T2} charges clamp capacitor C_c. At time t_1, the voltage u_{Cc} increases to the maximum and the current i_{LT2} becomes zero.

Model 2 *[t_1-t_2]:* The current i_{LT1} and i_{LT2} increases gradually, and the capacitor C_c charges the coil L_{T2} in reverse. At time t_2, the current i_{LT2} increases to the maximum.

Model 3 *[t_2-t_3]:* The current of Q_1 decreases to zero gradually, the capacitors C_c and C_2 are discharged through the coil L_{T2}, the voltage of capacitor C_{T1} decreases from input voltage to zero, the current of receiving coil L_R changes direction. At time t_3, the current i_{LT1} increases to the maximum.

Model 4 *[t_3-t_4]:* The low side switch Q_1 turns OFF, the voltage u_{CT1} increases in reverse, the capacitor C_2 and C_c continues to discharge, and the current i_{LT1} and i_{LT2} decrease. At time t_4, the voltage u_{C2} decreases to zero, the voltage u_{Cc} decreases to the minimum.

Model 5 *[t_4-t_5]:* The capacitor C_c begins to charge, and the transmitting coils L_{T1} and L_{T2} continue to discharge through the body diode of the high side switch Q_2. At time t_5, the gate-source voltage u_{gs2} becomes a high level, which achieves ZVS turn ON of high side switch Q_2.

Model 6 *[t_5-t_6]:* The high side switch Q_2 is turned ON, and the current reverses. The coils L_{T1} and L_{T2} charge the clamp capacitor C_c. At time t_6, the current i_{LT2} decreases to zero.

Model 7 *[t_6-t_7]:* The current of Q_2 increases positively, the clamp capacitor C_c continues to charge, and the coil L_{T2} begins to charge in reverse, while the coil L_{T1} continues to discharge. At time t_7, the current i_{LT1} and i_{Cc} decrease to zero.

Model 8 *[t_7-t_8]:* The current i_{LT1} and i_{Cc} increase in reverse, the coil L_{T2} continues to charge, and the current of receiving coil L_R changes direction. At time t_8, the current i_{LT2} increases to the maximum.

Model 9 *[t_8-t_9]:* The current of Q_2 decreases to zero gradually, the coil L_{T2} charges the capacitors C_c, C_2 and the coil L_{T1}.The capacitor C_{T1} discharges positively. At time t_9, the voltage u_{CT1} increases to the zero.

Model 10 *[t_9-t_{10}]:* The high side switch Q_2 turns OFF, the voltage u_{CT1} increases positively, the coils L_{T1} and L_{T2} together charge capacitors C_2 and C_c. At time t_{10}, the voltage u_{CT1} increases to the input voltage.

Model 11 *[t_{10}-t_{11}]:* The coils L_{T1} and L_{T2} continue to charge the capacitor C_c through the body diode of the low side switch Q_1. At time t_{11}, the current i_{LT1} decreases to zero, and the voltage u_{gs1} becomes a high level, which achieves ZVS turn ON of low side switch Q_1.

III. Design of the Proposed Two-Coil Driving Circuit

Fig. 4(a) and (b) shows the equivalent circuit models of the proposed two-coil driving circuit when Q_1 is on or Q_2 is ON. Here, Z_1 and Z_2 are the reflection impedances of the receiving circuit, r_{T1} and r_{T2} are the internal resistances of the L_{T1} and L_{T2}.

Assume that the receiver satisfies the full resonance condition, i.e., $\omega L_R = 1/\omega L_R$, then Z_1 and Z_2 can be expressed as

$$\begin{cases} Z_1 = \frac{(\omega M_1 \pi)^2}{8R + r_R} \\ Z_2 = \frac{(\omega M_2 \pi)^2}{8R + r_R} \end{cases} \tag{1}$$

where r_R is the internal resistances of the L_R.

As can be seen from the operation process in Section II, if the transmitter adopts the full compensation approach, the low side switch Q_1 is equivalently connected in parallel with a large capacitor, which does not allow for a wide range of ZVS and drive the coil with large inductance. Therefore, the analysis and design of the proposed two-coil driving circuit is given in this section, in terms of power distribution between two coils, output voltage with misalignment, ZVS operation, and parameter design.

A. Power Distribution of TX Coils

In order to drive the power distribution between two transmitting coils, the two equivalent models in Fig. 4 are analyzed.

According to Fig. 4(a), when the low side switch Q_1 is ON, i.e., $(-dT, D_1T)$ time, the current i_{LT1} and i_{LT2} continues to increase, the state equation at this stage can be expressed as follows:

$$\begin{cases} i_{LT1}(t)(Z_1 + r_{T1}) + L_{T1}\frac{di_{LT1}(t)}{dt} = U_{dc} \\ i_{LT2}(t)(Z_2 + r_{T2}) + L_{T2}\frac{di_{LT2}(t)}{dt} + u_{CT2}(t) = -u_{Cc}(t) \\ i_{LT2}(t) = C_{T2}\frac{du_{CT2}(t)}{dt} = C_{Cc}\frac{du_{Cc}(t)}{dt}. \end{cases} \tag{2}$$

At time t_0, the initial current $i_{LT1}(dT) = 0$, and $i_{LT1}(t)$ in this stage can be derived

$$i_{LT1}(t) = \frac{U_{dc}}{Z_1 + r_{T1}}\left(1 - e^{-\frac{(Z_1 + r_{T1})(t - dT)}{L_{T1}}}\right). \tag{3}$$

Besides, the initial and end values of the current i_{LT1} in this stage, i.e., the minimum and maximum values can be expressed as $I_1 = I_{L1\_min} = i_{LT1}(0)$ and $I_2 = I_{L1\_max} = i_{LT1}((D_1+d)T)$.

According to Fig. 4(b), when the high side switch Q_2 is ON, i.e., $((D_1+d)T, T)$ time, the current i_{LT1} and i_{LT2} continues to

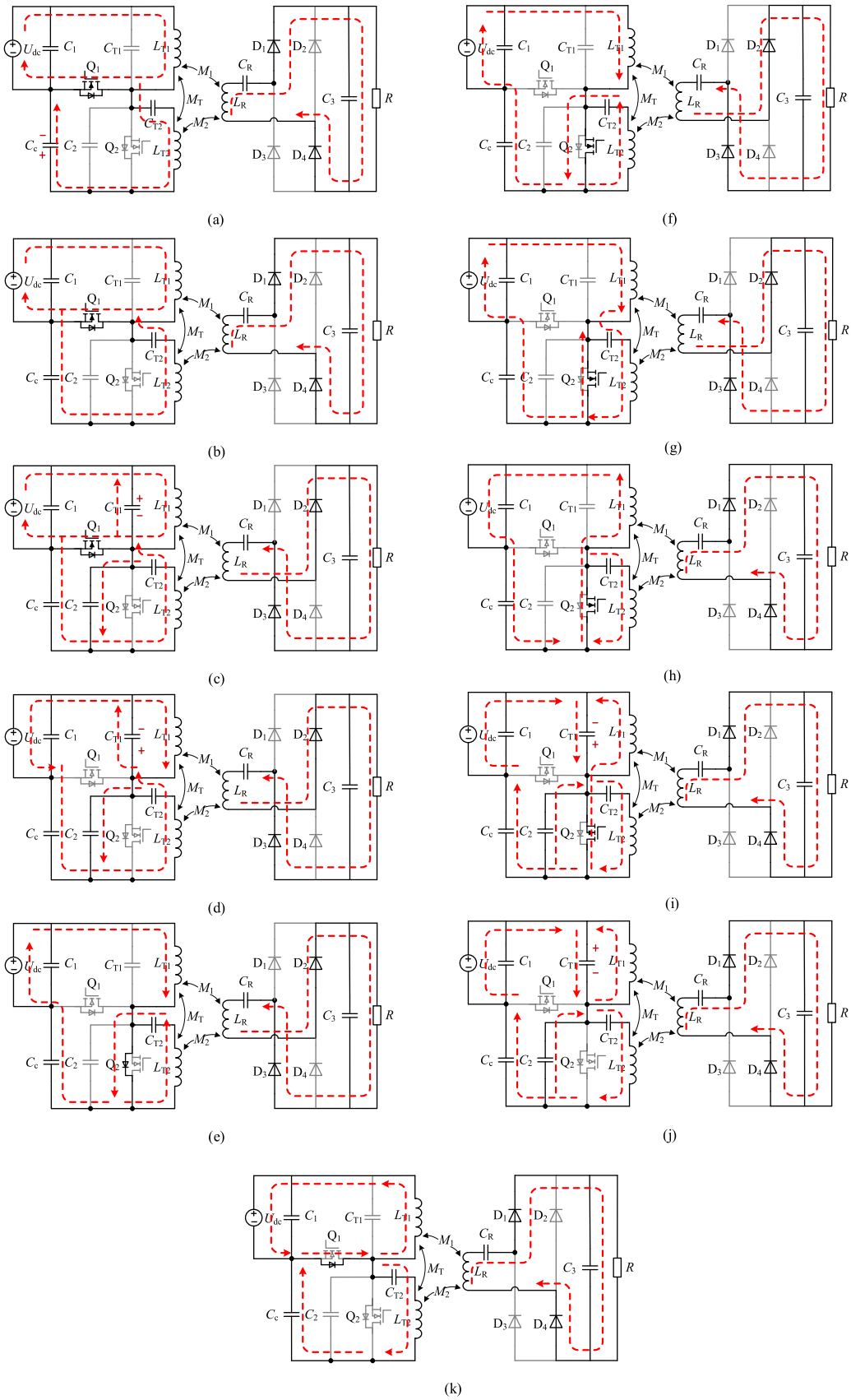

Fig. 3. Operation process. (a) Mode1 [t_0-t_1]. (b) Mode2 [t_1-t_2]. (c) Mode3 [t_2-t_3]. (d) Mode4 [t_3-t_4]. (e) Mode5 [t_4-t_5]. (f) Mode6 [t_5-t_6]. (g) Mode7 [t_6-t_7]. (h) Mode8 [t_7-t_8]. (i) Mode9 [t_8-t_9]. (j) Mode10 [t_9-t_{10}]. (k) Mode 11 [t_{10}-t_{11}].

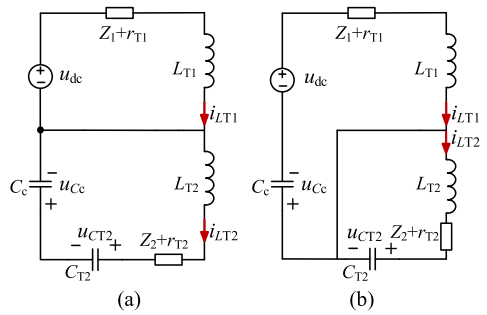

Fig. 4. Equivalent model of the two-coil driving circuit. (a) When Q_1 is ON. (b) When Q_2 is ON.

decrease, the state equation at this stage can be expressed as follows:

$$\begin{cases} i_{LT1}(t)(Z_1+r_{T1}) + L_{T1}\frac{\mathrm{d}i_{LT1}(t)}{\mathrm{d}t} + u_{Cc}(t) = U_{dc} \\ i_{LT2}(Z_2+r_{T2}) + L_{T2}\frac{\mathrm{d}i_{LT2}(t)}{\mathrm{d}t} + u_{CT2}(t) = 0 \\ i_{LT1}(t) = C_c\frac{\mathrm{d}u_{Cc}(t)}{\mathrm{d}t} \\ i_{LT2}(t) = C_{T2}\frac{\mathrm{d}u_{CT2}(t)}{\mathrm{d}t}. \end{cases} \tag{4}$$

For simplification purpose, the initial time $t_3 = (D_1+d)T$ at this state taken as zero time, and $i_{LT1}(t)$ in this stage can be obtained

$$i_{LT1}(t) = C_c\lambda_1 A_1 e^{\lambda_1 t} + C_c\lambda_2 A_2 e^{\lambda_2 t} \tag{5}$$

where A_1 and A_2 are the coefficients. According to the initial and end values of the current i_{LT1}, A_1, and A_2 can be expressed

$$\begin{cases} \lambda_1 = -\frac{Z_1+r_{T1}}{2L_{T1}}, \lambda_2 = \sqrt{\frac{(Z_1+r_{T1})^2C_c-4L_{T1}}{4L_{T1}^2C_c}} \\ A_1 = \frac{I_2e^{\lambda_2(D_2+d)T}-I_1}{C_c\lambda_1\left(e^{\lambda_2(D_2+d)T}-e^{\lambda_1(D_1+d)T}\right)} \\ A_2 = \frac{I_2e^{\lambda_1(D_2+d)T}-I_1}{C_c\lambda_2\left(e^{\lambda_1(D_2+d)T}-e^{\lambda_2(D_2+d)T}\right)}. \end{cases}$$

Because of the large capacitance of the clamp capacitor C_c, the average voltage U_{Cc} can be solved by using the volt-second balance characteristic according to the equivalent circuit in Fig. 4. The steady-state equation of the circuit can be expressed as

$$\begin{cases} U_{dc} = (Z_1+r_{T1})i_{LT1+} + L_{T1}\frac{i_{LT1+}}{(D_1+d)T} \\ U_{dc}-U_{Cc} = -(Z_1+r_{T1})i_{LT1-} - L_{T1}\frac{i_{LT1-}}{(D_2+d)T}. \end{cases} \tag{6}$$

Since $\Delta i_{LT1+} = \Delta i_{LT1-}$, the voltage U_{Cc} can be solved by (6)

$$U_{Cc} = U_{dc}\frac{1}{1-(D_1+d)}. \tag{7}$$

With U_{Cc} as a special solution, the voltage $u_{Cc}(t)$ can be solved as follows:

$$u_{Cc}(t) = A_1e^{\lambda_1 t} + A_2e^{\lambda_2 t} + U_{Cc} - A_1e^{\lambda_1(D_2+d)T} - A_2e^{\lambda_2(D_2+d)T}. \tag{8}$$

Similarly, the initial and end values of $u_{Cc}(t)$ at this stage are expressed as $U_{Cc1} = u_{Cc}(0)$, and $U_{Cc2} = U_{Cc} = u_{Cc}((D_2+d)T)$.

According to (2), the voltage $u_{Cc}(t)$ and $i_{LT2}(t)$ at stage Q_1-ON can be obtained

$$\begin{cases} u_{Cc}(t) = Ae^{\alpha t}\sin(\beta t+\varphi)+N \\ i_{LT2}(t) = AC_c\sqrt{\alpha^2+\beta^2}e^{\alpha t}\cos(\beta t+\varphi+\gamma) \end{cases} \tag{9}$$

where $\begin{cases} \alpha = -\frac{(Z_2+r_{T2})}{2L_{T2}}, \gamma = \arctan(\frac{\alpha}{\beta}) \\ \beta = \sqrt{\frac{4L_{T2}(C_c+C_{T2})-(Z_2+r_{T2})^2C_cC_{T2}}{4C_cC_{T2}L_{T2}^2}}. \end{cases}$

Based on the boundary value of $u_{Cc}(t)$ and the average value of current $i_{LT2}(t)$ as 0, the parameter relationship can be derived

$$\begin{cases} A\sin\varphi + N = U_{Cc} \\ Ae^{\alpha(D_1+d)T}\sin(\beta(D_1+d)T+\varphi)+N = U_{Cc1} \\ i_{LT2}(0) = -i_{LT2}((D_1+d)T). \end{cases} \tag{10}$$

From (10), A, φ and N can be expressed as follows:

$$\begin{cases} \varphi = \arctan\left(\frac{e^{-\alpha(D_1+d)T}+\cos(\beta(D_1+d)T)}{\sin(\beta(D_1+d)T)}\right)-\gamma \\ A = \frac{U_{Cc}-U_{C1}}{\sin\varphi-e^{\alpha(D_1+d)T}\sin(\beta(D_1+d)T+\varphi)}. \\ N = U_{Cc}-A\sin\varphi \end{cases}$$

The initial and end values of the current i_{LT2} in stage Q_1-ON, i.e., the minimum and maximum values can be expressed as $I_3 = I_{L2\_min} = i_{LT2}(0)$ and $I_4 = I_{L2\_max} = i_{LT2}((D_1+d)T)$.

According to (4), the current $i_{LT2}(t)$ at stage Q_2-ON can be obtained

$$i_{LT2}(t) = A_3C_{T2}\sqrt{\alpha_1^2+\beta_1^2}e^{\alpha_1 t}\cos(\beta_1 t+\varphi_1+\gamma_1) \tag{11}$$

where $\begin{cases} \alpha_1 = -\frac{Z_2+r_{T2}}{2L_{T2}}, \beta_1 = \sqrt{\frac{4L_{T2}-(Z_2+r_{T2})^2C_{T2}}{4L_{T2}^2C_{T2}}} \\ \gamma_1 = \arctan(\alpha_1/\beta_1) \\ \varphi_1 = \arctan\left(\frac{I_4\cos(\beta_1(D_2+d)T)-I_3e^{-\alpha(D_2+d)T}}{I_4\sin(\beta_1(D_2+d)T)}\right)-\gamma_1 \\ A_3 = \frac{I_4}{C_{T2}\sqrt{\alpha_1^2+\beta_1^2}\cos(\varphi_1+\gamma_1)}. \end{cases}$

In order to achieve wide range of ZVS and driving large inductor coils, the impedance of the low side switch in parallel needs to realize weak inductance, so the capacitor C_{T2} only compensates part of L_{T2}, which allows a dc component in the voltage of capacitor C_{T2}, i.e., the average voltage U_{CT2}. From Fig. 4, the steady-state equation can be also obtained

$$\begin{cases} U_{Cc} = U_{CT2} + (Z_2+r_{T2})i_{LT2+} + L_{T2}\frac{i_{LT2+}}{(D_1+d)T} \\ 0 = U_{CT2} - L_{T2}\frac{i_{LT2-}}{(D_2+d)T} - (Z_2+r_{T2})i_{LT2+}. \end{cases} \tag{12}$$

Since $\Delta i_{LT2+} = \Delta i_{LT2-}$, the voltage U_{CT2} can be solved by (10)

$$U_{CT2} = U_{Cc}(D_1+d). \tag{13}$$

With U_{CT2} as a special solution, the voltage $u_{CT2}(t)$ can be solved by (4) as follows:

$$u_{CT2}(t) = A_3e^{\alpha_1 t}\sin(\beta_1 t+\varphi_1) + U_{CT2} - A_3\sin(\varphi_1). \tag{14}$$

According to (3), (5), (9), and (11), the rms values of the fundamental components of i_{LT1} and i_{LT2} are defined as I_{LT1_rms}

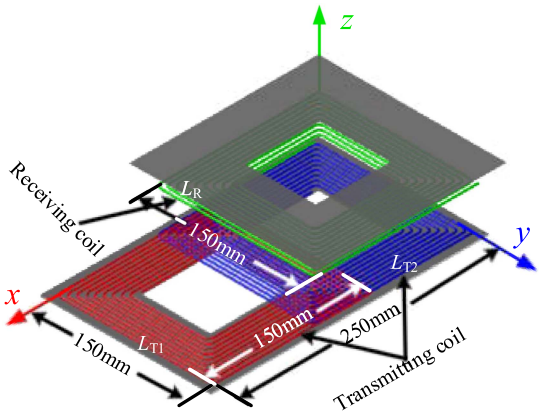

Fig. 5. Bipolar coil for the two-coil driving circuit.

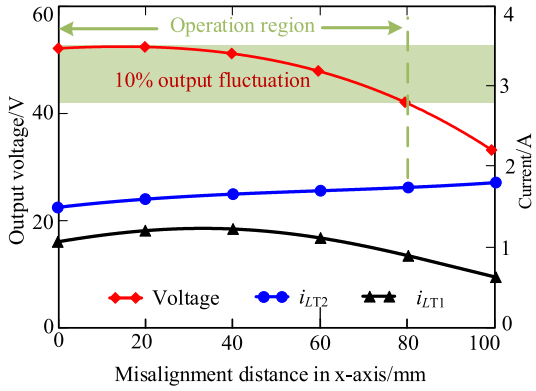

Fig. 6. Variation of output voltage and coils current with misalignment distance in x-axis.

and I_{LT2_rms}, respectively, as shown in

$$I_{LT1\_rms} = \sqrt{\frac{1}{T}\int_T i_{LT1}(t)\, e^{-\mathrm{j}\left(\frac{2\pi}{T}\right)t}\mathrm{d}t}$$

$$I_{LT2\_rms} = \sqrt{\frac{1}{T}\int_T i_{LT2}(t)\, e^{-\mathrm{j}\left(\frac{2\pi}{T}\right)t}\mathrm{d}t}. \tag{15}$$

So, the power distribution ratio of coils L_{T1} and L_{T2} is expressed as

$$r = \frac{P_{L1}}{P_{L2}} = \frac{I_{LT1\_rms}^2 Z_1}{I_{LT2\_rms}^2 Z_2}. \tag{16}$$

It can be seen from (16) that the power distribution of transmitting coils is mainly determined by rms current and mutual inductances between transmitting and receiving coils. The rms value of the two transmitting coils current depends on the corresponding duty cycle.

B. Output Voltage With Misalignment

In order to improve the misalignment tolerance of the WPT system when the duty cycle is constant, a bipolar transmitter with two independent coils is adopted, and a square coil is used for the receiving coil, as shown in Fig. 5. In addition, a 50 mm overlap between the two transmitter coils allows for decoupling of the magnetic field.

It can be seen from Fig. 5 that when the receiving coil L_R moves along the x-axis, the mutual inductance M_2 between L_R and L_{T2} will gradually decrease, while the mutual inductance M_1 between L_R and L_{T1} will gradually increase. The starting coordinate is defined as the vertex of coil L_{T2}, where the receiving coil is completely aligned with coil L_{T2}. The total voltage of the WPT system can be expressed as

$$U_o \approx \sqrt{(P_{L1} + P_{L2})\, R}$$

$$= \sqrt{\left(\frac{U_{CT1}^2}{Z_1^2 + \omega^2 L_{T1}^2} Z_1 + \frac{U_{C2}^2}{Z_2^2 + \omega^2 L_2^2} Z_2\right) R} \tag{17}$$

where L_2 is the remaining equivalent inductance with C_{T2} and L_{T2} compensation. When the misalignment distance ranges from 0 to 10 cm, mutual inductance M_1 gradually increases and M_2 gradually decreases, which means the varying trend of the reflected impedance Z_1 and Z_2 is opposite. From the analysis of the circuit, it can be seen that U_{CT1} and U_{C2} remain basically unchanged while the duty cycle remains constant. Therefore, under the designed parameters, P_{L1} increases with the increase of Z_1, and P_{L2} decreases with the decrease of Z_2, which overall helps compress the output voltage variation caused by the misalignment.

Similarly, according to (17), as the load R increases, Z_1 and Z_2 decrease, resulting in the increased P_{L1} and the decreased P_{L2} and then small change in the output voltage U_o.

Assuming that the change ratio of mutual inductance is fixed with the increase of misalignment distance, the variation of output voltage and coils current with misalignment distance in x-axis is shown in Fig. 6. (The circuit parameters used in the following figures are shown in Table I.)

It can be seen from Fig. 6 that under constant duty cycle, the output voltage fluctuation of the circuit is not more than 10% within the 80 mm misalignment distance in x-axis.

When the x-axis of the coil is aligned and the duty cycle of two switches is 0.4, the variation of output voltage and coils current

TABLE I
PARAMETERS OF TWO-COIL DRIVING CIRCUIT

Symbol	Definition	Value
f	frequency	1 MHz
U_{dc}	Input dc voltage	100 V
U_o	Output voltage	50 V
$L_{T1}(L_{T2})$	Transmitting coil inductance	16.8 μH
L_R	Receiving coil inductance	17.15 μH
M_1	Range of mutual inductance	0.5–5.15 μH
M_2	Range of mutual inductance	4.92–0.58 μH
C_R	Receiving compensation capacitor	1.48 nF
C_{T1}	L_{T1} compensation capacitor	300 pF
C_{T2}	L_{T2} compensation capacitor	2.8 nF
C_2	Compensation capacitor	300 pF
C_c	Active clamp capacitor	200 nF

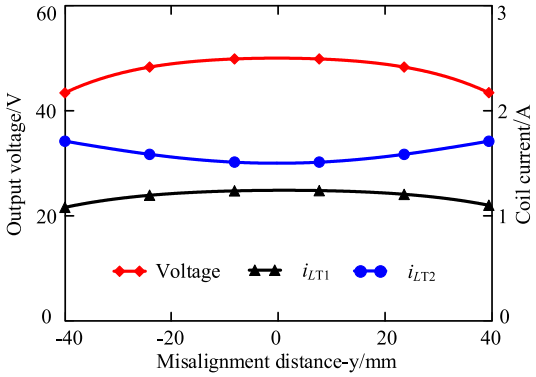

Fig. 7. Variation of output voltage and coils current with misalignment distance in y-axis.

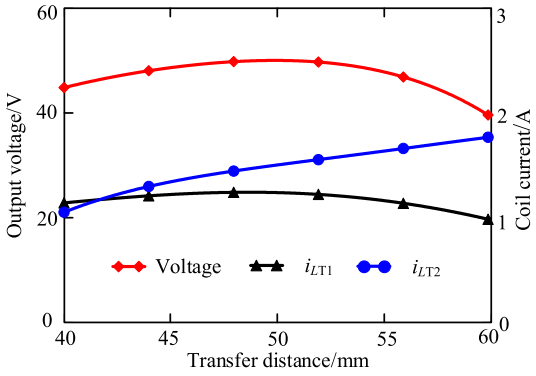

Fig. 8. Curves of output voltage and coils current with transfer distance.

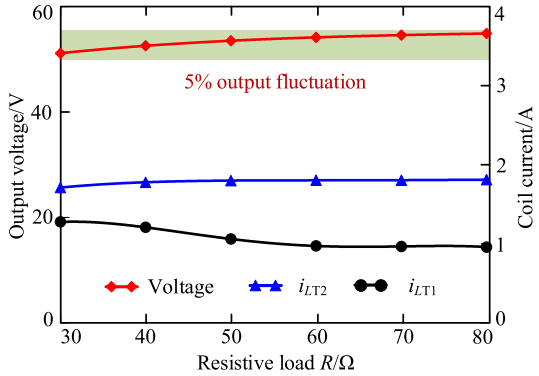

Fig. 9. Variation of output voltage and coil current with resistive load.

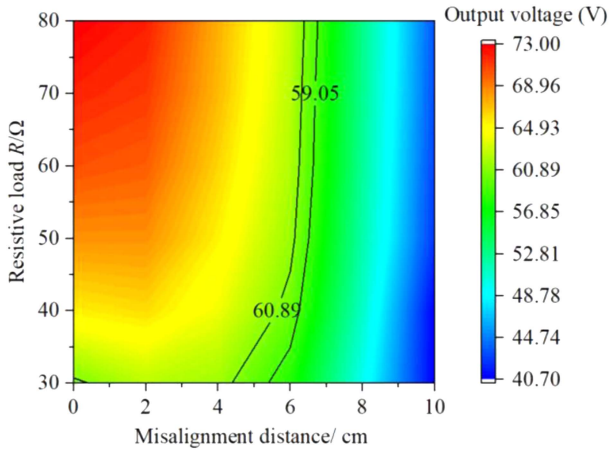

Fig. 10. Fluctuation of output voltage with the change of misalignment and load.

with misalignment distance in y-axis is shown in Fig. 7. From Fig. 7, it can be seen that the output voltage and coil current are symmetrical when the y-axis is misaligned.

When the x-axis and y-axis of the coil is aligned and the duty cycle of two switches is 0.4, the curves of transmit coil current and output voltage with transfer distance are shown in Fig. 8.

From Fig. 8, it can be seen that when the transmission distance is 5 cm, the output voltage is the highest. This is because a closer transmission distance will result in the loss of ZVS, while a further distance will result in a smaller mutual inductance.

The curves of transmit coil current and output voltage with load under constant mutual inductance ($M_1 = 2.4\ \mu$H, $M_2 = 3.57\ \mu$H) and duty cycle ($D_1 = D_2 = 0.4$) are shown in Fig. 9.

As can be seen from Fig. 9, when the load is swept from 30 to 80 Ω, the output voltage fluctuates within a range of 5%, and the larger the load resistance, the more constant the output voltage.

For the determined duty cycle ($D_1 = 0.5$, $D_2 = 0.3$), the fluctuation of output voltage when the system faces with both misalignment (After that the misalignment is all in x-axis) and load variation is given, as shown in Fig. 10. It can be seen from Fig. 10 that the larger resistive load, the greater impact of misalignment distance on the output voltage. In addition, the larger the misalignment distance, the smaller impact on the output voltage when the load changes. Therefore, load changes need to be considered in parameter design.

Moreover, when the load changes from 30 to 80 Ω and the misalignment distance from 0 to 10 cm, the output voltage varies from 40 to 73 V at the duty cycle of 0.4. In order to achieve a constant voltage of 50 V, the output voltage varies between −23 V and 10 V, i.e., the system needs to have a regulation capability of 27–60 V.

C. Analysis of the ZVS Operation

In order to achieve the ZVS operation for the low side and high side switches, it is necessary to optimize the capacitance of C_{T1}, C_{T2}, and C_2. Since the voltage on C_2 is approximately rectangular wave, to achieve a smaller reactive power circulation, C_{T2} is required to compensate part of L_{T2}, thus presenting an inductive impedance. This inductance presented after compensation is defined as L_2, which needs to meet

$$L_2 \geq \frac{U_{C\mathrm{T2}} M_2}{\sqrt{P_{\mathrm{o}} R}} \tag{18}$$

where P_{o} is output power of the system.

In addition, C_{T2} can be expressed as

$$C_{\mathrm{T2}} = \frac{1}{\omega^2 \left(L_{\mathrm{T2}} - L_2\right)}. \tag{19}$$

However, too large L_2 will lead to more reactive power in the circuit, which will affect the system output power, so it is only necessary to meet (18) and (19) under the maximum mutual inductance M_2 during design. Setting the current $i_{LT1}(dT)$ and

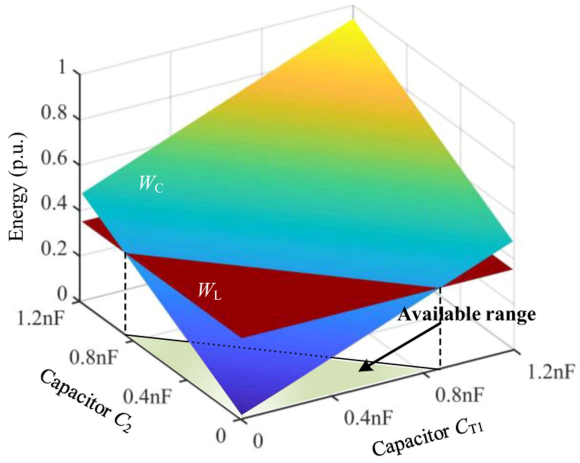

Fig. 11. Relationship between energy and capacitors.

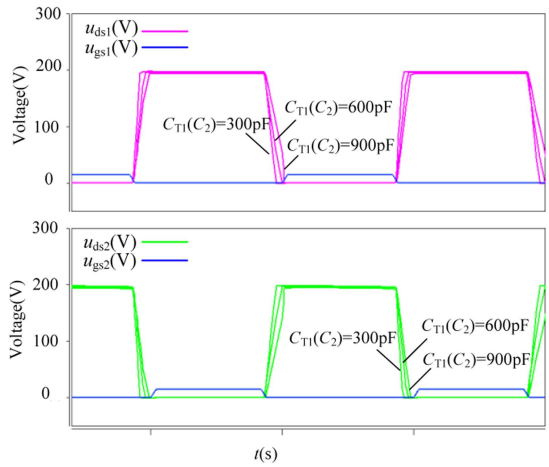

Fig. 12. Switch voltage waveforms at different capacitors.

$i_{LT2}(dT)$ are less than zero, the conditions for achieving ZVS can be derived. Here, the energy approach is used for design.

According to the theoretical analysis, the energy of the inductor is greater than the energy of the capacitor C_{T1} and C_2 in the dead time, which can realize the ZVS of the two switches. Therefore, the condition can be obtained as follow in (20).

When the duty cycle is fixed, the relationship between energy and capacitors is shown in Fig. 11.

As can be seen from Fig. 11, the capacitor energy is less than the inductor energy when the capacitors C_{T1} and C_2 are in the available range, which can achieve reliable ZVS

$$W_L = \frac{1}{2}\left(L_{T1} i_{LT1}(0)^2 + L_2 i_{LT2}(0)^2\right) > W_C = \frac{1}{2}\left(C_2 U_{CT2}^2 + C_{T1} U_{dc}^2 + C_{T1}(U_{Cc} - U_{dc})^2\right) \quad (20)$$

where W_L and W_C are the energy of inductors and capacitors, respectively.

Fig. 12 shows the voltage waveform of the switches Q_1 and Q_2 with different capacitors C_{T1} and C_2 at constant duty cycle. It can be seen that with the increase of capacitance, the ZVS margin becomes smaller, and it is difficult for the low side switch to realize ZVS than the high side switch.

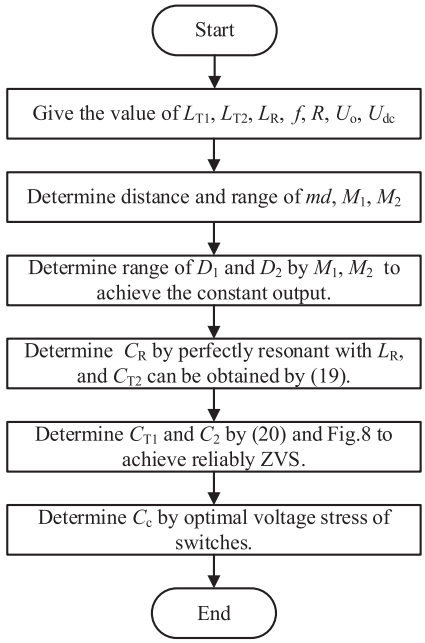

Fig. 13. Flow chart of parameter design.

D. Parameter Design

According to the abovementioned analysis, the parameter design process of the two-coil driving circuit is summarized and shown in Fig. 13.

First, the parameters of the transmitting and receiving coils and the input and output voltages need to be given. Second, based on the actual coils to determine the transmission distance, and the variation range of misalignment distance (md) and mutual inductance (M_1, M_2). Third, the duty cycle of the switches is determined according to the variation range of mutual inductance to ensure the constant output voltage. Then, the capacitor C_R can be obtained by L_R, and the capacitor C_{T2} can be determined by (19). Next, the capacitors C_{T1} and C_2 need to satisfy (20) and can be obtained from Fig. 11 to achieve ZVS. Finally, the clamp capacitor C_c is designed by switch voltage stress to achieve optimal cost.

In this article, the two-coil driving circuit is applied to portable devices, i.e., wireless charging for one or more devices such as computers, tablets, phones, and headphones. With the measured coils parameter, the relationship between D_1, D_2 and output voltage is given, as shown in Fig. 14. [Light green is the area where the duty cycle is not applicable, and the dead time duty cycle is half of (1-D_1-D_2)]. It can be seen from Fig. 14 that the output voltage is positively correlated with the duty cycle of the low side switch at constant mutual inductor, so the voltage can be adjusted only by changing the duty cycle of the low side switch.

From Fig. 14 that the voltage variation range is between 27 V and 72 V, which can meet the voltage variation shown in Fig. 10.

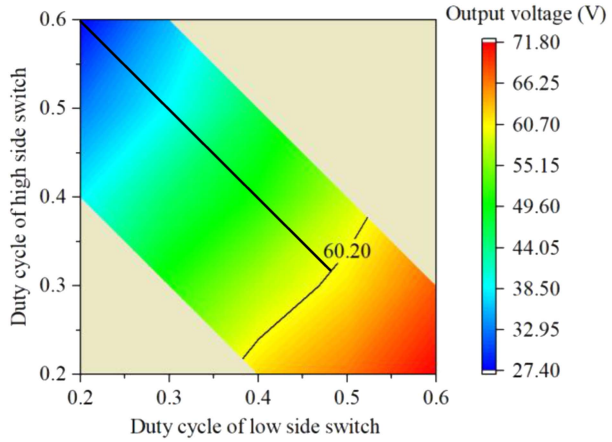

Fig. 14. Relationship between output voltage and duty cycle.

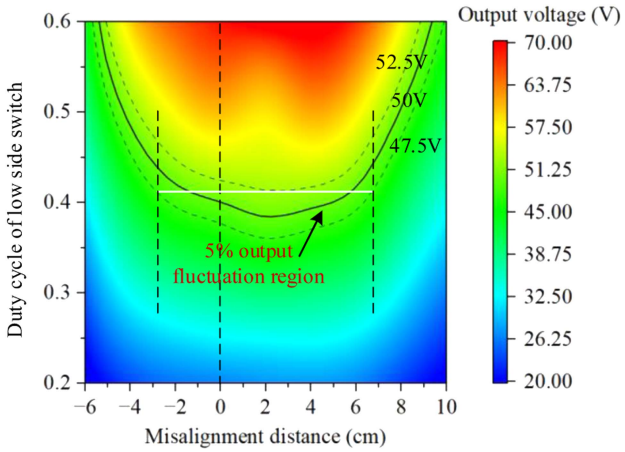

Fig. 15. Relationship of U_o with the change of *md* and D_1.

The duty cycle of the low side switch can be adjusted from 0.2 to 0.48 along the black line to achieve a constant output voltage.

Based on the design process in Fig. 13, the parameters of the proposed circuit are given and listed in Table I. (The coil parameters are the measured value.)

IV. Simulation and Experiment Verification

According to the parameters listed in Table I, the simulation shows that the relationship of output voltage with the change of misalignment distance and duty cycle of low side switch is, as shown in Fig. 15.

The area between the dotted lines is the 5% output fluctuation region. As can be seen in Fig. 15, with a fixed duty cycle, a misalignment distance between −3 cm and 7 cm can achieve an output voltage within 5% fluctuation. In addition, with the low side switch duty cycle changes between 0.4 and 0.6, the output fluctuation can be achieved within 5% at the misalignment distance from −6 to 10 cm.

In order to validate the proposed two-coil driving circuit and the misalignment tolerance of the system, a 1 MHz wireless power transfer prototype with 50 V constant voltage is built, as shown in Fig. 16.

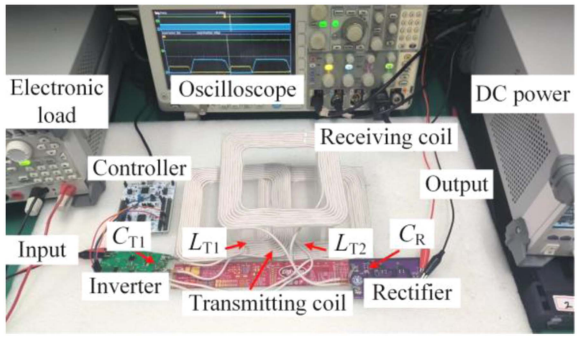

Fig. 16. Experimental prototype of the proposed WPT system.

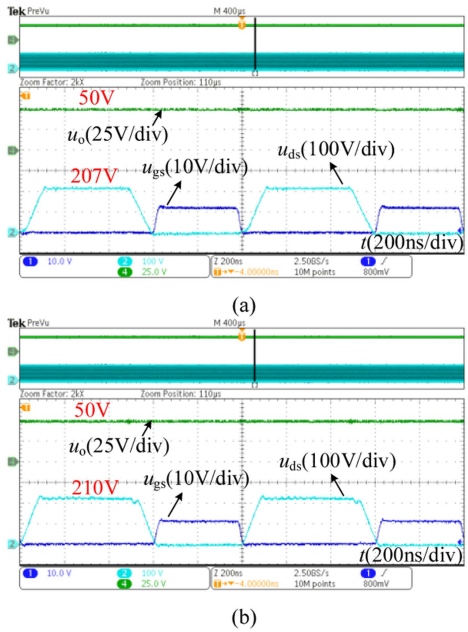

Fig. 17. ZVS waveform of two switches with coil aligned at 0.4 duty cycle. (a) Low side switch. (b) High side switch.

Fig. 17(a) and (b) shows the gate driving and drain-source voltage waveforms of the low side switch and the high side switch when the L_R and L_{T2} are well aligned.

At this time, the duty cycle of both low side switch and high side switch is 0.4. It can be seen that both the low side and high side switches achieve zero-voltage turn-ON, with about 210 V switch voltage stress and 50 V output voltage, which meets the design demand.

When the duty cycle remains constant, the relationship between the output voltage (U_o) and the coil misalignment distance(*md*) at *x*-direction is shown in Table II.

As can be seen from Table II, when the coil is misaligned in the positive direction, the output voltage first increases and then decreases due to the increase of mutual inductance with coil L_{T1}. When the coil is misaligned in negative direction, the output voltage decreases with the increase of the misalignment distance. In addition, the output voltage fluctuation within 5% can be achieved within −3 to 6 cm coil misalignment distance.

TABLE II
OUTPUT VOLTAGE WITH MISALIGNMENT DISTANCE

md(cm)	-6	-4	-2	0
U_o(V)	31.4	42.5	47.9	50
md(cm)	2	4	6	8
U_o(V)	51.6	50.8	48	41.1

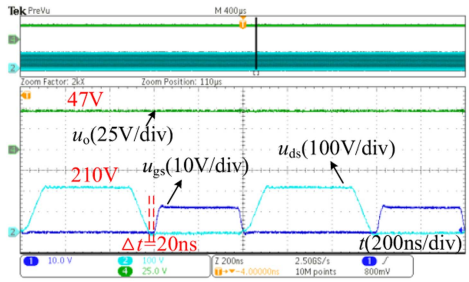

Fig. 18. ZVS waveform of low side switch with 6 cm coil misalignment.

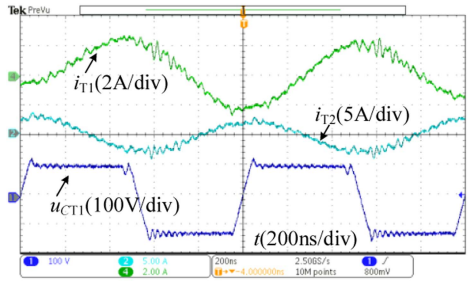

Fig. 19. Two transmitting coil currents and capacitor voltage.

When the coil misalignment distance is about 6 cm, the ZVS waveform of the low side switch is shown in Fig. 18. It can be seen from that both the ZVS margin and the switch voltage stress increase after coil misalignment, and the output voltage decreases by 5% at a misalignment distance of 6 cm.

Besides, the two transmitting coil currents and the voltage of the capacitor C_{T1} are shown in Fig. 19. It can be seen that the experimental waveform is basically consistent with the theoretical waveform in Fig. 2, which verifies the correctness of the topology and analysis.

In order to achieve a constant output voltage with coil misalignment, the duty cycle of the two switches is adjusted with a fixed dead time, e.g., a dead time of 0.1 T. When the coil misalignment distance is 6 cm, the output voltage and switch duty are shown in Fig. 20. It can be seen that the output voltage is stable at about 50 V, when the duty cycle of the low side switch and the high side switch are about 0.45 and 0.35, respectively, and the switch voltage stress becomes larger as the duty cycle of the low side switch increases.

When the coil misalignment distance is 9 cm, the output voltage and low side switch duty cycle waveforms can also be obtained, as shown in Fig. 21. It shows that the output voltage is still 50 V when the coil misalignment distance is 9 cm, and the switch achieves ZVS with a switch voltage stress of 350 V.

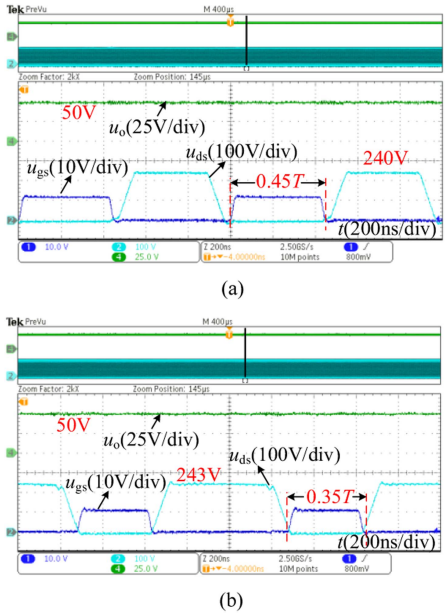

Fig. 20. Output voltage and switch duty cycle with coil misalignment 6 cm. (a) Low side switch. (b) High side switch.

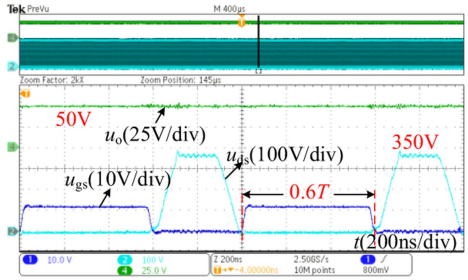

Fig. 21. Output voltage and low side switch duty cycle with coil misalignment 9 cm.

TABLE III
CHARACTERISTICS OF WPT SYSTEM AT DIFFERENT COIL MISALIGNMENT DISTANCES

Misalignment distance	Mutual inductance(M_1)	Mutual inductance(M_2)	Efficiency
-6 cm	0.3 μH	2.6 μH	84.5%
-4 cm	0.3 μH	3.71 μH	87.3%
-2 cm	0.16 μH	4.58 μH	87.9%
0	0.5 μH	4.92 μH	88.7%
2 cm	1.25 μH	4.45 μH	89.4%
4 cm	2.4 μH	3.57 μH	89%
6 cm	4.07 μH	2.45 μH	88.3%
8 cm	4.68 μH	1.47 μH	87.1%
10 cm	5.15 μH	0.58 μH	85.2%

The experimental results show that when the low side switch duty cycle is adjusted between 0.4 and 0.6, the output voltage fluctuation within 5% can be achieved within -6 cm to 10 cm coil misalignment distance. Reliable ZVS can be achieved within the range of -6 cm to 10 cm. This is because the entire

TABLE IV
PERFORMANCE COMPARISON WITH OTHER APPROACHES

	Coil type	Coil size(cm)	Number of switches /coils	Compensation component	Efficiency and power	Misalignment range(cm) (percentage)	Output fluctuation	Load change	Limitation of the coils current
Proposed	BP	25×15	2(3)	3	89.4%/80W	-6~+10(40%)	5%	CV	Yes
[10]	QDQ	40×40	4(4)	8	93.9%/3.5kW	±15 (37.5%)	5%	CV	Yes
[24]	DD	73.8×39.1	4(4)	6	94%/3.3kW	-8~+12 (16.3%)	5%	CC	Yes
[25]	DD	73.8×39.1	4(4)	8	91.5%/3.3kW	±15 (38.4%)	10%	CC	No
[26]	IPTS	90×110	4(4)	5	75%/15kW	±40 (36.4%)	29%	CC	No
[27]	DD	45×45	4(4)	6	94.8%/3.7kW	±15 (33.3%)	43.2%	No	Yes
[28]	TCC	Diameter=42	4(3)	4	90.1%/680W	±10 (23.8%)	39.26%	CV	Yes
[29]	BP	60×60	4(4)	5	96.7%/3.3kW	±30 (50%)	5%	CC	Yes
[30]	Multi	28×28	4(3)	3	81%/200W	±14 (50%)	8.6%	CC	No

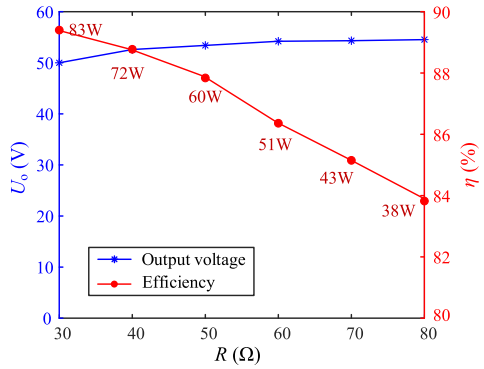

Fig. 22. Output voltage and efficiency of the system at constant duty cycle.

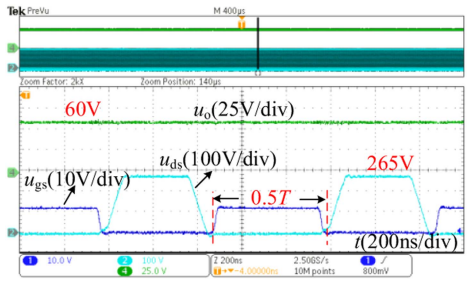

Fig. 23. Output voltage and switch duty cycle with coil aligned.

misalignment distance can achieve ZVS is taken into account when designing C_2 and C_{T1}.

When the output voltage fluctuates within 5%, the characteristics of WPT system at different misalignment distances are shown in Table III.

As can be seen from Table III, the maximum efficiency of the system is about 89.4%, which occurs at the position of 2 cm of misalignment distance. In addition, when the load is swept from 30 to 80 Ω, the output voltage and efficiency of the system at constant duty cycle is shown in Fig. 22.

As shown in Fig. 22, the output voltage remains basically constant as the load resistance varies between 30 and 80 Ω, while the efficiency decreases as the load resistance increases. This is because as the load resistance increases, the power gradually decreases, while the coil current changes slightly, resulting in a decrease in efficiency. Therefore, when the load resistance changes, the switch duty cycle only needs to be adjusted slightly to achieve the constant output voltage. In addition, ZVS can be achieved when the load resistance is greater than 25 Ω. And the larger the resistance, the easier it is to achieve ZVS.

For the proposed circuit, the switch voltage stress remains unchanged without changing the input voltage and duty cycle, so higher power output can be achieved according to design needs.

When the circuit parameters remain unchanged, the coil aligned, and the duty cycle of Q_1 is increased from 0.4 to 0.5, the out power can reach 120 W and its waveform is given in Fig. 23.

In order to present the superiority of the proposed two-coil driving circuit in terms of misalignment tolerance and component count, the proposed circuit has been compared with other approaches, as shown in Table IV.

It can be seen from Table IV that the proposed scheme has low component count, i.e., switches, coils, and compensation component. Generally speaking, the higher the power, the higher the efficiency will be relatively, because the inherent losses account for a smaller percentage. At the same power level, compared with [28] and [30], this proposed circuit has a significant advantage in efficiency. Moreover, compared with the methods [10], [24], [25], [26], [27], [28], the proposed approach in this article has better misalignment tolerance, and the output can achieve load independent. Compared with [29], [30], the proposed approach has a little bit smaller misalignment range, but has few switches and coils.

V. Conclusion

In this article, a WPT system with a two-coil driving circuit is proposed for high misalignment tolerance and low component count. Adopting two decoupled coils as the bipolar transmitter, the proposed circuit can control each coil individually for power distribution, thus ensuring a fixed total output voltage against high misalignment. The design approach is given in the paper for reliable ZVS with a wide range of coil misalignment and load variations. Experimental results show that a constant output voltage can be achieved with a coil misalignment of −6 cm to 10 cm, when the duty cycle of the switches only needs to change from 0.4 to 0.6.

References

[1] Y. Yao, Y. Wang, X. Liu, F. Lin, and D. Xu, "A novel parameter tuning method for a double-sided LCL compensated WPT system with better comprehensive performance," *IEEE Trans. Power Electron.*, vol. 33, no. 10, pp. 8525–8536, Oct. 2018.

[2] Y. Chen, S. He, B. Yang, S. Chen, Z. He, and R. Mai, "Reconfigurable rectifier-based detuned series-series compensated IPT system for anti-misalignment and efficiency improvement," *IEEE Trans. Power Electron.*, vol. 38, no. 2, pp. 2720–2729, Feb. 2023.

[3] Y. Bi et al., "Modified deadbeat predictive current control method for single-phase AC–DC PFC converter in EV charging system," *IEEE Trans. Ind. Electron.*, vol. 70, no. 1, pp. 286–297, Jan. 2023.

[4] J. Feng, Q. Li, F. C. Lee, and M. Fu, "Transmitter coils design for free-positioning omnidirectional wireless power transfer system," *IEEE Trans. Ind. Inform.*, vol. 15, no. 8, pp. 4656–4664, Aug. 2019.

[5] C. Liu, C. Jiang, J. Song, and K. T. Chau, "An effective sandwiched wireless power transfer system for charging implantable cardiac pacemaker," *IEEE Trans. Ind. Electron.*, vol. 66, no. 5, pp. 4108–4117, May 2019.

[6] Z. Wei, B. Zhang, S. Lin, and C. Wang, "A self-oscillation WPT system with high misalignment tolerance," *IEEE Trans. Power Electron.*, to be published, doi: 10.1109/TPEL.2023.3327096.

[7] K. Song et al., "A rotation-lightweight wireless power transfer system for solar wing driving," *IEEE Trans. Power Electron.*, vol. 34, no. 9, pp. 8816–8830, Sep. 2019.

[8] T. Kan, R. Mai, P. P. Mercier, and C. C. Mi, "Design and analysis of a three-phase wireless charging system for lightweight autonomous underwater vehicles," *IEEE Trans. Power Electron.*, vol. 33, no. 8, pp. 6622–6632, Aug. 2018.

[9] M. Itraj and W. Ettes, "Topology study for an inductive power transmitter for cordless kitchen appliances," in *Proc. IEEE PELS Workshop Emerg. Technol., Wireless Power Transfer*, 2018, pp. 1–8.

[10] Y. Chen et al., "A hybrid inductive power transfer system with misalignment tolerance using quadruple-D quadrature pads," *IEEE Trans. Power Electron.*, vol. 35, no. 6, pp. 6039–6049, Jun. 2020.

[11] Y. Chen et al., "A clamp circuit-based inductive power transfer system with reconfigurable rectifier tolerating extensive coupling variations," *IEEE Trans. Power Electron.*, to be published, doi: 10.1109/TPEL.2023.3303487.

[12] H. Pang, K. T. Chau, W. Han, W. Liu, and Z. Zhang, "Decoupled-double D coils based dual-resonating-frequency compensation topology for wireless power transfer," *IEEE Trans. Magn.*, vol. 58, no. 2, Feb. 2022, Art. no. 8000407.

[13] M. Budhia, J. T. Boys, G. A. Covic, and C.-Y. Huang, "Development of a single-sided flux magnetic coupler for electric vehicle IPT charging systems," *IEEE Trans. Ind. Electron.*, vol. 60, no. 1, pp. 318–328, Jan. 2013.

[14] A. Zaheer, H. Hao, G. A. Covic, and D. Kacprzak, "Investigation of multiple decoupled coil primary pad topologies in lumped IPT systems for interoperable electric vehicle charging," *IEEE Trans. Power Electron.*, vol. 30, no. 4, pp. 1937–1955, Apr. 2015.

[15] A. Ahmad, M. S. Alam, and A. A. S. Mohamed, "Design and interoperability analysis of quadruple pad structure for electric vehicle wireless charging application," *IEEE Trans. Transp. Electrific.*, vol. 5, no. 4, pp. 934–945, Dec. 2019.

[16] G. Ke, Q. Chen, W. Gao, S.-C. Wong, C. K. Tse, and Z. Zhang, "Research on IPT resonant converters with high misalignment tolerance using multicoil receiver set," *IEEE Trans. Power Electron.*, vol. 35, no. 4, pp. 3697–3712, Apr. 2020.

[17] S. Kim, G. A. Covic, and J. T. Boys, "Tripolar pad for inductive power transfer systems for EV charging," *IEEE Trans. Power Electron.*, vol. 32, no. 7, pp. 5045–5057, Jul. 2017.

[18] Y. Li, T. Lin, R. Mai, L. Huang, and Z. He, "Compact double-sided decoupled coils-based WPT systems for high-power applications: Analysis, design, and experimental verification," *IEEE Trans. Transp. Electrific.*, vol. 4, no. 1, pp. 64–75, Mar. 2018.

[19] C. Zhu and W. Zhong, "Small-signal modeling and decoupling control method of modular WPT systems," *IEEE Trans. Power Electron.*, vol. 38, no. 6, pp. 7863–7876, Jun. 2023, doi: 10.1109/TPEL.2023.3244161.

[20] Q. Zhang et al., "Research on input-parallel single-switch wireless power transfer system with constant-current and constant-voltage output," *IEEE Trans. Power Electron.*, vol. 37, no. 4, pp. 4817–4830, Apr. 2022.

[21] X. Zhang, Y. Zhang, Z. Zhang, and M. Li, "Mode conversion and structure optimization of quadrature coils for electric vehicles wireless power transfer," *IEEE Trans. Energy Convers.*, vol. 35, no. 2, pp. 575–590, Jun. 2020.

[22] X. Qu, Y. Yao, D. Wang, S.-C. Wong, and C. K. Tse, "A family of hybrid IPT topologies with near load-independent output and high tolerance to pad misalignment," *IEEE Trans. Power Electron.*, vol. 35, no. 7, pp. 6867–6877, Jul. 2020.

[23] X.-J. Ge, Y. Sun, Z.-H. Wang, and C.-S. Tang, "Dual-independent-output inverter for dynamic wireless power transfer system," *IEEE Access*, vol. 7, pp. 107320–107333, 2019.

[24] L. Zhao, D. J. Thrimawithana, U. K. Madawala, A. P. Hu, and C. C. Mi, "A misalignment-tolerant series-hybrid wireless EV charging system with integrated magnetics," *IEEE Trans. Power Electron.*, vol. 34, no. 2, pp. 1276–1285, Feb. 2019.

[25] L. Zhao, D. J. Thrimawithana, and U. K. Madawala, "Hybrid bidirectional wireless EV charging system tolerant to pad misalignment," *IEEE Trans. Ind. Electron*, vol. 64, no. 9, pp. 7079–7086, Sep. 2017.

[26] S. Y. Choi, J. Huh, W. Y. Lee, and C. T. Rim, "Asymmetric coil sets for wireless stationary EV chargers with large lateral tolerance by dominant field analysis," *IEEE Trans. Power Electron.*, vol. 29, no. 12, pp. 6406–6420, Dec. 2014.

[27] F. Lu, H. Zhang, H. Hofmann, W. Su, and C. C. Mi, "A dual-coupled LCC-compensated IPT system with a compact magnetic coupler," *IEEE Trans. Power Electron.*, vol. 33, no. 7, pp. 6391–6402, Jul. 2018.

[28] C. Zhang, Y. Yao, and Y. Wang, "Decoupling optimization of the three-coil coupler for IPT system featuring high efficiency and misalignment tolerance," *IEEE Trans. Ind. Electron.*, vol. 70, no. 9, pp. 8918–8927, Sep. 2023, doi: 10.1109/TIE.2022.3215831.

[29] G. Li, Z. Yao, S. Luo, and H. Ma, "A hybrid IPT system implementing misalignment tolerance and constant current output with primary intermediate coil," *IEEE J. Emerg. Sel. Topics Power Electron.*, vol. 10, no. 6, pp. 7797–7807, Dec. 2022.

[30] Z. Yuan, M. Saeedifard, C. Cai, Q. Yang, P. Zhang, and H. Lin, "A misalignment tolerant design for a dual-coupled LCC-S-compensated WPT system with load-independent CC output," *IEEE Trans. Power Electron.*, vol. 37, no. 6, pp. 7480–7492, Jun. 2022.

Houji Li (Student Member, IEEE) was born in Taian, China, in 1996. He received the B.S. and M.S. degrees from Qingdao University, Qingdao, China, in 2017 and 2020, respectively. He is currently working toward the Ph.D. degree with Shanghai Jiao Tong University, Shanghai, China, all in electrical engineering.

His current research interests include wireless power transfer and high frequency power electronics.

Dr. Li was the recipient of the Best Student Paper Prize of IEEE WoW in 2021.

Zhan Liu (Student Member, IEEE) was born in Xuchang, China, in 1999. He received the B.S. degree from Harbin Institute of Technology, Harbin, China, in 2020. He is currently working toward the M.S. degree with Shanghai Jiao Tong University, Shanghai, China, both in electrical engineering.

His current research interests include MHz inductive power transfer and high frequency magnetic component fabrication.

Bo Pan was born in Shaoxing, China, in 1990. He received the B.S. degree from Jinan University, Guangzhou, China, in 2013, and the M.S. degree from Shanghai Maritime University, Shanghai, China, in 2016. He is currently working toward the Ph.D. degree with Shanghai Jiao Tong University, Shanghai, China, all in electrical engineering.

He is currently with Shanghai Aerospace Technology Research Institute. His current research interests include aerospace project management and wireless power transfer.

Wei Liu (Graduate Student Member, IEEE) received the B.Sc. degree from the Changsha University of Science and Technology, Changsha, China, in 2019, and the M.S. degree from Southwest Jiao Tong University, Chengdu, China, in 2019. He is currently working toward the Ph.D degree with Shanghai Jiao Tong University, Shanghai, China, all in electrical engineering.

His main research interest includes on high-frequency power converter circuits.

Jian Wang received the B.S. degree in electrical engineering from North China Electric Power University, Beijing, China, in 2018. She is currently working toward the Ph.D. degree with the Department of Electrical Engineering, Shanghai Jiao Tong University, Shanghai, China. She is currently working toward the Ph.D. degree with the Energy Department, Politecnico di Milano, Milan, Italy.

Her research interests include optimal operation of virtual power plant and integrated energy system.

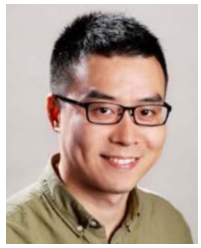

Ming Liu (Senior Member, IEEE) received the B.S. degree in mechatronic engineering from Sichuan University, Chengdu, China, in 2007, and the Ph.D. degree in electrical and computer engineering from the University of Michigan-Shanghai Jiao Tong University Joint Institute, Shanghai Jiao Tong University, Shanghai, China, in 2017.

From 2017 to 2020, he was a Postdoctoral Research Fellow with the Department of Electrical Engineering, Princeton University, Princeton, NJ, USA. In 2020, he was with the School of Electronic Information and Electrical Engineering, Shanghai Jiao Tong University, where he is currently an Associate Professor of electrical engineering. His research interests include megahertz wireless power transfer, battery management systems, and high frequency high performance power electronics for emerging applications.

Dr. Liu was the recipient of the Top Ten Academic Star Award and the Excellent Ph.D. Thesis Award Nomination from the Shanghai Jiao Tong University, in 2016 and 2018, the Research Excellence Award from AirFuel Alliance, USA, in 2019, the Best Paper Award of IEEE Energy Conversion Congress and Exposition-Asia in 2020, and the Best Student Paper Prize of IEEE WoW in 2021 with his student. He is the Chair of the Wireless Power Transfer for Energy Storage Charging Subcommittee of Energy Storage Technical Committee, IEEE Industrial Electronics Society.

Yong Wang (Member, IEEE) received the Ph.D. degree in power electronics from Zhejiang university, Hangzhou, China, in 2005.

From 2005 to 2008, he was a Senior Researcher in Samsung Advanced Institute of Technology, Suwon, South Korea, working on the fuel cell grid tied inverter. From 2008 to 2010, he was with Danfoss Solar Inverters, Soenderborg, Denmark, as a power electronics Hardware Engineer. In the year 2010, he was with Shanghai Jiao Tong University, Shanghai, China, where he is currently a Full Professor with the Department of Electrical Engineering. His main research interests include grid-tied inverter technology, high frequency dc–dc converter based on wide bandgap devices applied in EV, and wireless power transfer.